NASA TECHNICAL NOTE

NASA TN D-4359

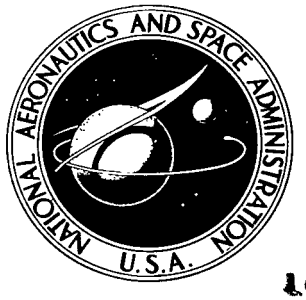

NASA TN D-4359

VEHICLE ATTITUDE DETERMINATION WITH A SINGLE ONBOARD CAMERA

by Richard J. Bendura, Allen B. Henning, and Robert E. Smith, Jr.

Langley Research Center
Langley Station, Hampton, Va.

NATIONAL AERONAUTICS AND SPACE ADMINISTRATION • WASHINGTON, D. C. • MARCH 1968

VEHICLE ATTITUDE DETERMINATION WITH A SINGLE ONBOARD CAMERA

By Richard J. Bendura, Allen B. Henning, and Robert E. Smith, Jr.

Langley Research Center
Langley Station, Hampton, Va.

NATIONAL AERONAUTICS AND SPACE ADMINISTRATION

For sale by the Clearinghouse for Federal Scientific and Technical Information
Springfield, Virginia 22151 – CFSTI price $3.00

VEHICLE ATTITUDE DETERMINATION WITH A SINGLE ONBOARD CAMERA

By Richard J. Bendura, Allen B. Henning,
and Robert E. Smith, Jr.
Langley Research Center

SUMMARY

Application of a postflight photographic method for determining the attitude history of a vehicle equipped with a single onboard camera is presented. Also included is an appendix showing the equation and geometric relationships of the method. For application, a minimum of two earth-related points need be identified on each photograph and the location of the vehicle with respect to the earth must be determined. In addition, the orientation of the camera axes system with respect to the vehicle is required. The method requires no other onboard instrumentation.

The method was applied in determining the spacecraft attitude for a portion of the first flight test of the Planetary Entry Parachute Program (PEPP). The spacecraft was equipped with two relatively lightweight and inexpensive 16-mm motion-picture cameras which photographed the surface of the earth. Data were obtained for altitudes ranging from 130 000 to 143 000 feet (40 to 44 kilometers). A comparison is made of the results independently obtained from each camera with ground-based tracking data and with an azimuth datum point from an onboard magnetometer direction finding system.

INTRODUCTION

For many flight projects, data would be more meaningful if a time history of vehicle attitude could be obtained. Various instruments such as accelerometers, gyro platforms, rate gyros, horizon sensors, and cameras have been used singly and in combination to define vehicle attitude. Of the cameras used, most have been restricted to highly sophisticated and expensive systems which are capable of obtaining very accurate results. However, for some flight applications such accuracy is not necessary. Where vehicle orientation angles within several degrees are sufficient, photographs from an inexpensive camera not designed as a metric instrument may be used. In reference 1 a method of vehicle attitude determination with a single onboard camera is shown for a special case in which the horizon and one identifiable landmark are available on each

photograph. References 2 and 3 present an analysis requiring a minimum of four landmarks assumed to be at the same elevation in order to determine vehicle attitude.

The data presented in this report were obtained by means of 16-mm motion-picture cameras which were intended only to photograph the deployment of an experimental parachute (refs. 4 and 5). However, during analysis of the data, it was noticed that throughout a large portion of the flight several landmarks could be identified on the film. This provided an opportunity for determining the spacecraft attitude history – in this case through application of a camera orientation method. The appendix presents the equations for the camera orientation method used in this investigation and is intended to serve as a guide for future applications. The method requires a minimum of two landmarks within view of the camera, location of the camera with respect to the landmarks, and orientation of the vehicle with respect to the camera.

SYMBOLS

c	focal length of camera
h	height above sea level of camera, feet (meters)
I	point in image space
K	constant of proportionality between object space coordinate system and image space coordinate system
n	number of observations
Q	point in object space
R	geocentric earth radius, feet (meters)
t	flight time, seconds
X,Y,Z	object space coordinate axes with origin at focal point; also, distance along these axes, feet (meters)
$\overline{X},\overline{Y},\overline{Z}$	distance from geocentric coordinate axes origin, feet (meters)
X_E,Y_E,Z_E	earth-fixed axes system

X_I, Y_I, Z_I image space coordinate axes with origin at focal point

$\bar{x}, \bar{y}$ measured image coordinates in image space coordinate system

$\bar{x}_p, \bar{y}_p$ coordinates of point of intersection between focal plane and focal axes in image space coordinate system

γ_p spacecraft flight-path angle measured in X_E, Z_E plane, degrees

γ_y spacecraft flight-path angle measured in X_E, Y_E plane, degrees

$\Delta\sigma$ change in attitude angle

ϵ error in $\bar{x}$

$\bar{\epsilon}$ error in $\bar{y}$

Λ longitude of camera measured positive east from Greenwich, degrees

$\left.\begin{matrix}\lambda_1, \mu_1, \nu_1 \\ \lambda_2, \mu_2, \nu_2 \\ \lambda_3, \mu_3, \nu_3\end{matrix}\right\}$ directional cosines of image space coordinate system relative to object space coordinate system

σ_e attitude angles with random error for error analysis, degrees

σ_{th} theoretical attitude angles for error analysis, degrees

$\sigma_1, \sigma_2, \sigma_3$ camera azimuth, pitch, and roll Euler angles relative to earth-fixed axes, degrees

Φ geodetic latitude of camera measured positive north, degrees

Φ' geocentric latitude of camera measured positive north, degrees

ψ, θ, ϕ spacecraft azimuth, pitch, and roll Euler angles relative to earth-fixed axes, degrees

Subscripts:

i for camera $i = 1$ and for object space points $i = 2 \ldots n + 1$

o initial conditions

S spacecraft

Superscript:

T transposing of matrix

CAMERA ORIENTATION METHOD

In order to determine the orientation of a camera used to photograph the surface of the earth, the following are required: the photographic or image coordinates of at least two identification points such as mountain peaks, river bends, and so forth; the earth coordinates of these identification points; and the location of the camera with respect to the earth. The coordinate system defining both the earth-related identification points and the camera is referred to as the object space coordinate system. The photographic coordinate system defined by the camera focal axis and the focal plane in which the coordinates of the images of the identification points may be measured is called the image space coordinate system. In order to determine the camera orientation, it is necessary to determine the relationship between these two coordinate systems. A detailed discussion of the mathematical relationships between corresponding points in the image space coordinate system and the object space coordinate system is presented in the appendix. A least-squares solution to the relationship between the two coordinate systems is also shown. The resulting equations can be easily programed into a digital computer system.

APPLICATION OF METHOD

The camera orientation method described in the preceding section was applied to determine the spacecraft attitude during a portion of the first balloon-launched flight test of the Planetary Entry Parachute Program (ref. 4). The test took place at White Sands Missile Range, New Mexico. The spacecraft, shown in figure 1, was a 15-ft-diameter (4.6 m) 60° half-angle cone. It contained two 16-mm motion-picture cameras which are relatively lightweight and inexpensive when compared to other cameras used in photogrammetry. Moreover, the cameras were not intended to be used as metric instruments; instead they were placed on the spacecraft to photograph the inflation characteristics of an experimental parachute (ref. 5). Each camera was equipped with a lens having a focal length of 10.5 mm, a field of view of 38° by 52°, and a maximum radial distortion of less than 2 percent. They were mounted in the base of the spacecraft and were pointed toward the ground during the ascending portion of the trajectory.

The geodetic coordinates and altitude of the identification points were determined by comparing 10- by 7-cm enlargements of the 16-mm frames with a 1:250 000 scale contour map. Prominent geographical areas such as mountain ranges and rivers were readily identified which established the general region being photographed. Further study of the enlargements enabled more minute geographical details such as mountain tops and the intersection of rivers to be discerned.

The relationship between the spacecraft and camera axis systems was fixed prior to launch. The cameras were mounted in the base of the aeroshell, pointed aft, and rotated 15° from the nominal vertical.

A total of 170 frames from the two cameras were enlarged and studied for possible landmarks which could be used as identification points. After identification of the landmarks, the 16-mm film was placed in a film reader which enlarged the film by a factor of 20. The coordinates of the identification points with respect to the film (or image space) were located and automatically punched on data processing cards. In order to increase reading accuracy each point was read three times and the average value of these readings was used.

From two to five landmarks were located and used as identification points on each frame investigated. A total of 12 landmarks were identified but only 10 were used in this application. The earth coordinates of these points are given in table I. Figure 2 shows the location of the identification points on a map overlapping the northwest corner of the White Sands Missile Range. Enlargements of three of the 16-mm frames analyzed with the identification points marked are shown in figure 3. These points are numbered and can be compared with the corresponding points of table I and figure 2.

The appendix presents the equations which relate the points on earth or object space with points on the film or image space. The equations were set up in matrix form and solved on a digital computer. The results were then transformed from the camera angle orientation system given by σ_1, σ_2, and σ_3 (fig. 4) to the spacecraft attitude system given by ψ, θ, and ϕ (fig. 5).

The relationship between the two orientation systems for this particular application is as follows:

$$\psi = \sigma_1 - 180^{\circ}$$

$$\theta = -\sigma_2$$

$$\phi = -\left(\sigma_3 + 15^{\circ}\right)$$

The data are presented in terms of both the camera orientation system and the spacecraft attitude system.

The primary purpose of the spacecraft cameras during the PEPP flight test was to obtain parachute deployment data and not spacecraft attitude data. Therefore, no attempt was made to assure that the focal axes of the cameras were parallel to either the longitudinal axis of the spacecraft or to each other. Subsequent comparison of the film indicated that the focal axes of the two cameras were misalined 5^{o} relative to each other. After reviewing the assembly procedures and spacecraft drawings, it was estimated that the focal axis of each camera could vary as much as 6^{o} with the spacecraft longitudinal axis.

ACCURACY

A Monte Carlo error analysis was performed to determine the accuracy of the camera attitude angles. One hundred frames having two or three observation points were forced to be theoretically errorless by adjusting the photographic image coordinates to a zero residual condition. (See appendix.) Normally distributed random errors with mean zero and expected standard deviation in each of the parameters in the system were introduced into the theoretical case and new solutions obtained. The sources of error considered (and the corresponding deviations) were

(1) Locating the coordinates of the identification points on the 16-mm film (±100 microns)

(2) Determining the latitude, longitude, and altitude of the identification points (±0.5 minutes and ±60 meters)

(3) Locating the spacecraft by ground-based tracking instrumentation (±60 meters)

(4) Measuring the focal length of the camera (±1.5 microns)

(5) Locating the center of the frame (±10 microns)

Ten cases having random error selection were employed for each frame. The camera attitude angle variances were computed by using the following equation:

$$\Delta\sigma_i^2 = \frac{\sum_{j=1}^{\eta} \left(\sigma_{e,ij} - \sigma_{th,i}\right)^2}{\eta - 3}$$

where

$i = 1, 2, 3$

$\eta = 10$

Histograms of the variances of each angle for the 100 frames were plotted and 95-percent confidence regions established. The results indicate that σ_1 is known within $\pm 1.5^{\circ}$, σ_2 within $\pm 1.0^{\circ}$, and σ_3 within $\pm 3.3^{\circ}$.

RESULTS AND DISCUSSION

Data were obtained from both cameras during 28 seconds of the flight test covering an altitude range from 130 000 to 143 000 feet (40 to 44 kilometers). Beyond this time the spacecraft flight path was nearly horizontal and the cameras were pointed away from the surface of the earth.

Time histories of the camera orientation Euler angles σ_1, σ_2, and σ_3 (fig. 4) and the aeroshell attitude Euler angles ψ, θ, and ϕ (fig. 5) are presented in figures 6 to 8. Figure 6 compares the yaw-angle (σ_1 or ψ) results obtained from both cameras with ground tracking data and a point obtained from an onboard magnetometer. Pitch-angle (σ_2 or θ) results are compared with ground tracking data in figure 7 and roll-angle (σ_3 or ϕ) data are presented in figure 8.

At $t = 0$ the spacecraft was released from a balloon and fell toward earth until a cluster of rocket motors in the base of the spacecraft ignited at $t = 3.7$ seconds. The motors burned for about 3 seconds propelling the spacecraft to transonic velocities. At $t = 7$ seconds a parachute was deployed in a reefed condition and remained physically connected to the spacecraft until $t = 14.2$ seconds. After this time the spacecraft was in unencumbered free flight and, as shown in figures 6 to 8, its period of oscillation increased by a factor of approximately 1.5.

The Euler angle data from camera 2 agree quite well with the results from camera 1. Both the amplitude variation during corresponding half-cycles and the oscillation frequency are in agreement within the accuracy of this investigation. That the amplitudes of the curves at specific times vary by as much as 10° is attributed to the relative misalinement of the two cameras. A 5° axes misalinement entirely in the $X_I - Z_I$ plane (fig. 4) of the camera, at a time when the spacecraft pitch angle was 60° and the roll angle was near zero, would result in a yaw-angle variation of about 10°. Such a situation exists during the time period from 0 to 3.67 seconds as shown in figure 6.

The camera results are compared with ground tracking data. Radar and optical tracking station data were combined to yield flight-path angles γ_y and γ_p in the yaw (X_E, Y_E) and pitch (X_E, Z_E) planes, respectively. These data are represented by the dashed lines beginning at 6 seconds in figures 6 and 7. The radar and optical tracking stations tracked the spacecraft as a point mass and, therefore, did not obtain the oscillatory attitude variations recorded by the two onboard cameras. Nevertheless, the camera Euler angles σ_1 and σ_2 (as well as ψ and θ) should oscillate about γ_y and

γ_p, respectively, in the absence of any wind. A fairing of the mean values of the camera data would not coincide with the ground track data. This is attributed to both the offset of the camera focal axis from the longitudinal axis of the spacecraft and the lateral velocity component of the spacecraft with respect to the ground caused by the wind. The prevailing winds during the portion of the flight test covered in this investigation were from an azimuth between 90^o and 110^o from north. The spacecraft, according to ground track data, flew at a flight-path angle γ_y of not less than 135^o. The resultant velocity vector would cause the mean values of σ_1 and ψ to be somewhat north of γ_y as shown in figure 6. In addition, because the winds were horizontal, the mean values of σ_2 and θ would be less than γ_p during the ascent portion of the trajectory as shown in figure 7.

CONCLUDING REMARKS

The use of a relatively unsophisticated onboard camera for postflight determination of vehicle attitude within an accuracy of $\pm 3.3^o$ has been demonstrated. The method employed requires

(1) The location of at least two identifiable objects within the view of the camera

(2) The location of the camera with respect to the objects being viewed

(3) The orientation of the vehicle with respect to the camera

The method does not require any other onboard instrumentation.

Langley Research Center,
National Aeronautics and Space Administration,
Langley Station, Hampton, Va., October 18, 1967,
124-07-03-05-23.

APPENDIX

PHOTOGRAMMETRIC DETERMINATION OF CAMERA ORIENTATION

In order to adequately describe how the camera orientation can be determined, it is necessary to define the coordinate systems in which observations are made. The coordinate system in which the position of observed points are known and in which the camera is oriented is called the object space. The coordinate system composed of the camera focal plane and focal axis and in which image coordinates are measured is the image space. (See ref. 6.) The relationship between a point in the object space and image space is

$$\left.\begin{aligned} \bar{x} - \bar{x}_p &= c\left(\frac{\lambda_1 X + \mu_1 Y + \nu_1 Z}{\lambda_3 X + \mu_3 Y + \nu_3 Z}\right) \\ \bar{y} - \bar{y}_p &= c\left(\frac{\lambda_2 X + \mu_2 Y + \nu_2 Z}{\lambda_3 X + \mu_3 Y + \nu_3 Z}\right) \end{aligned}\right\} \tag{A1}$$

The relationship in equations (A1) can be derived with the aid of figure 9. Let $Q(X,Y,Z)$ be a point in the object space, then the image of Q will be $I\left(X_I, Y_I, Z_I\right)$ in the image space. Since the origins of the two coordinate systems coincide for all practical purposes, the following transformation describes the coordinates of Q relative to the image space

$$\begin{bmatrix} X_I \\ Y_I \\ Z_I \end{bmatrix} = K \begin{bmatrix} \lambda_1 \mu_1 \nu_1 \\ \lambda_2 \mu_2 \nu_2 \\ \lambda_3 \mu_3 \nu_3 \end{bmatrix} \begin{bmatrix} X \\ Y \\ Z \end{bmatrix} \tag{A2}$$

where K is a constant of contraction. In equations (A2) dividing the first and second equations by the third equation removes the constant K and gives

$$\left.\begin{aligned} \frac{X_I}{Z_I} &= \frac{\lambda_1 X + \mu_1 Y + \nu_1 Z}{\lambda_3 X + \mu_3 Y + \nu_3 Z} \\ \frac{Y_I}{Z_I} &= \frac{\lambda_2 X + \mu_2 Y + \nu_2 Z}{\lambda_3 X + \mu_3 Y + \nu_3 Z} \end{aligned}\right\} \tag{A3}$$

Letting

$$\begin{aligned} \bar{x} - \bar{x}_p &= X_I \\ \bar{y} - \bar{y}_p &= Y_I \\ c &= Z_I \end{aligned}$$

and multiplying both sides of equations (A3) by c gives

$$\left.\begin{aligned} \bar{x} - \bar{x}_p &= c\left(\frac{\lambda_1 X + \mu_1 Y + \nu_1 Z}{\lambda_3 X + \mu_3 Y + \nu_3 Z}\right) \\ \bar{y} - \bar{y}_p &= c\left(\frac{\lambda_2 X + \mu_2 Y + \nu_2 Z}{\lambda_3 X + \mu_3 Y + \nu_3 Z}\right) \end{aligned}\right\} \tag{A4}$$

Equations (A4) are identical to equations (A1).

For each known point in the object space there exist two equations (A1) relating the object space to the image space. The directional cosines λ_1, μ_1, ν_1, . . ., of the image space axes relative to the object space axes can be expressed in terms of three angles σ_1, σ_2, and σ_3. Consequently, these angles can be used to describe the orientation of the camera coordinate system relative to the object space coordinate system. To obtain the directional cosines consider three successive rotations through the angles σ_1, σ_2, and σ_3. Using figure 4 and imposing a constant of contraction for the camera, the following transformation is obtained:

$$\begin{bmatrix} \bar{x} - \bar{x}_p \\ \bar{y} - \bar{y}_p \\ c \end{bmatrix} = K \begin{bmatrix} -C\sigma_1 C\sigma_3 - S\sigma_1 S\sigma_2 S\sigma_3 & S\sigma_1 C\sigma_3 - C\sigma_1 S\sigma_2 S\sigma_3 & C\sigma_2 S\sigma_3 \\ C\sigma_1 S\sigma_3 - S\sigma_1 S\sigma_2 C\sigma_3 & -S\sigma_1 S\sigma_3 - C\sigma_1 S\sigma_2 C\sigma_3 & C\sigma_2 C\sigma_3 \\ S\sigma_1 C\sigma_2 & C\sigma_1 C\sigma_2 & S\sigma_2 \end{bmatrix} \begin{bmatrix} X \\ Y \\ Z \end{bmatrix} = K \begin{bmatrix} \lambda_1 \mu_1 \nu_1 \\ \lambda_2 \mu_2 \nu_2 \\ \lambda_3 \mu_3 \nu_3 \end{bmatrix} \begin{bmatrix} X \\ Y \\ Z \end{bmatrix}.$$

where, for convenience, C and S represent cosine and sine, respectively. This equation is equivalent to equation (A2).

The Least-Squares Solution

The solution of equations (A1) contains six parameters which under theoretical conditions are constants. These parameters are $\bar{x}_p$, $\bar{y}_p$, c, σ_1, σ_2, and σ_3 of which $\bar{x}_p$, $\bar{y}_p$, and c are measured independently for this experiment and are not unknowns in the solution. A solution of equations (A1) for σ_1, σ_2, and σ_3 can be found with two properly chosen observations. Associated with $\bar{x}$ and $\bar{y}$ in equations (A1) are errors ϵ and $\bar{\epsilon}$. Since these errors exist, a computational method is needed which yields the best possible results with all the information available. The method of least squares which is described subsequently uses a minimum error criterion and has been used in the data reduction for this investigation.

APPENDIX

In general, equations (A1) with the associated errors can be written as

$$\left.\begin{aligned} \bar{x}_i &= F(\sigma_j) + \epsilon_i && (j = 1, 2, 3) \\ \bar{y}_i &= \overline{F}(\sigma_j) + \bar{\epsilon}_i && (i = 1, \ldots, n) \end{aligned}\right\} \tag{A5}$$

where F and $\overline{F}$ are nonlinear functions of σ_j and in order to find a solution they must be linearized. Expanding equations (A5) in a Taylor's series about a nominal set $\sigma_{j,o}$ and dropping the higher order terms results in the following linear approximations:

$$\left.\begin{aligned} \Delta\bar{x}_i &= \bar{x}_i - \bar{x}_{i,o} = b_{i1}(\sigma_1 - \sigma_{1,o}) + b_{i2}(\sigma_2 - \sigma_{2,o}) + b_{i3}(\sigma_3 - \sigma_{3,o}) + \epsilon_i \\ \Delta\bar{y}_i &= \bar{y}_i - \bar{y}_{i,o} = \bar{b}_{i1}(\sigma_1 - \sigma_{1,o}) + \bar{b}_{i2}(\sigma_2 - \sigma_{2,o}) + \bar{b}_{i3}(\sigma_3 - \sigma_{3,o}) + \bar{\epsilon}_i \end{aligned}\right\} \tag{A6}$$

where

$$b_{i1} = \left.\frac{\partial F_i}{\partial \sigma_1}\right|_{\sigma_{1,o}\sigma_{2,o}\sigma_{3,o}} \qquad \bar{b}_{i1} = \left.\frac{\partial \overline{F}_i}{\partial \sigma_1}\right|_{\sigma_{1,o}\sigma_{2,o}\sigma_{3,o}}$$

$$b_{i2} = \left.\frac{\partial F_i}{\partial \sigma_2}\right|_{\sigma_{1,o}\sigma_{2,o}\sigma_{3,o}} \qquad \bar{b}_{i2} = \left.\frac{\partial \overline{F}_i}{\partial \sigma_2}\right|_{\sigma_{1,o}\sigma_{2,o}\sigma_{3,o}}$$

$$b_{i3} = \left.\frac{\partial F_i}{\partial \sigma_3}\right|_{\sigma_{1,o}\sigma_{2,o}\sigma_{3,o}} \qquad \bar{b}_{i3} = \left.\frac{\partial \overline{F}_i}{\partial \sigma_3}\right|_{\sigma_{1,o}\sigma_{2,o}\sigma_{3,o}}$$

Letting

$$\Delta\sigma_j = (\sigma_j - \sigma_{j,o})$$

equations (A6) can be put in the following form:

$$\left.\begin{aligned} \Delta\bar{x}_i &= \sum_{j=1}^{3} b_{ij}\Delta\sigma_j + \epsilon_i \\ \Delta\bar{y}_i &= \sum_{j=1}^{3} \bar{b}_{ij}\Delta\sigma_j + \bar{\epsilon}_i \end{aligned}\right\} \quad (i = 1, \ldots, n) \tag{A7}$$

For further considerations the linear equations (A7) corresponding to the ith observation are expressed in matrix notation where

APPENDIX

$$v_i = B_i \Delta\sigma + e_i \tag{A8}$$

$$v_i = \begin{bmatrix} \Delta\bar{x}_i \\ \Delta\bar{y}_i \end{bmatrix} \qquad B_i = \begin{bmatrix} b_{i1} & b_{i2} & b_{i3} \\ \bar{b}_{i1} & \bar{b}_{i2} & \bar{b}_{i3} \end{bmatrix}$$

$$\Delta\sigma = \begin{bmatrix} \Delta\sigma_1 \\ \Delta\sigma_2 \\ \Delta\sigma_3 \end{bmatrix} \qquad e_i = \begin{bmatrix} \epsilon_i \\ \bar{\epsilon}_i \end{bmatrix}$$

Then for n observations there are n matrix equations of the form of equation (A8) which may be written

$$\overline{V} = \overline{B}\Delta\sigma + \bar{e} \tag{A9}$$

where

$$\overline{V} = \begin{bmatrix} v_1 \\ v_2 \\ \cdot \\ \cdot \\ \cdot \\ v_n \end{bmatrix} \qquad \overline{B} = \begin{bmatrix} B_1 \\ B_2 \\ \cdot \\ \cdot \\ \cdot \\ B_n \end{bmatrix} \qquad \bar{e} = \begin{bmatrix} e_1 \\ e_2 \\ \cdot \\ \cdot \\ \cdot \\ e_n \end{bmatrix}$$

The problem may be restated: given $\overline{V}$ and $\overline{B}$ find the best estimate $\widehat{\Delta\sigma}$ for $\Delta\sigma$.

The best estimate $\widehat{\Delta\sigma}$ is the value of $\widehat{\Delta\sigma}$ which minimizes the sum of the squares of the residuals $\bar{e}^T\bar{e}$ where

$$\bar{e}^T\bar{e} = \left(\overline{V} - \overline{B}\Delta\sigma\right)^T\left(\overline{V} - \overline{B}\Delta\sigma\right) \tag{A10}$$

In order to minimize equation (A10) the first variation δ with respect to $\Delta\sigma$ must vanish, that is

$$\left.\begin{aligned} \delta\left(\bar{e}^T\bar{e}\right) &= \delta\left[\left(\overline{V} - \overline{B}\Delta\sigma\right)^T\left(\overline{V} - \overline{B}\Delta\sigma\right)\right] = 0 \\ \delta\left(\bar{e}^T\bar{e}\right) &= -2\left(\overline{V}^T - \Delta\sigma^T\overline{B}^T\right)\overline{B}\delta\Delta\sigma = 0 \end{aligned}\right\} \tag{A11}$$

Since $\delta\Delta\sigma \neq 0$, equations (A11) can be satisfied if

$$\left(\overline{V}^T - \Delta\sigma^T\overline{B}^T\right)\overline{B} = 0$$

or

$$\overline{B}^T\overline{B}\Delta\sigma = \overline{B}^T\overline{V} \tag{A12}$$

Solving for the estimate of $\Delta\sigma$ in equation (A12) gives

$$\widehat{\Delta\sigma} = \left(\overline{B}^T\overline{B}\right)^{-1}\overline{B}^T\overline{V} \tag{A13}$$

A second necessary condition for equation (A10) to be a minimum is that the second variation with respect to $\Delta\sigma$ be positive definite. Upon examination the second variation is

$$\delta^2\left(\bar{e}^T\bar{e}\right) = 2\delta\Delta\sigma^T\overline{B}^T\overline{B}\delta\Delta\sigma$$

which is positive definite. Therefore, equation (A13) is a valid expression for $\widehat{\Delta\sigma}$.

Since equation (A13) is based on a linear approximation with nominal $\sigma_{j,o}$, $\widehat{\Delta\sigma}$ can be used to find the best estimates $\hat{\sigma}_j$. With the relationship $\sigma = \sigma_o + \Delta\sigma$, the value of $\widehat{\Delta\sigma}$ which minimized equation (A10) leads to a new nominal $\sigma_{j,o} = \sigma_{j,o} + \widehat{\Delta\sigma}$. This process implies an iterative procedure which continues until $\widehat{\Delta\sigma} \to 0$ and the value of $\sigma_{j,o}$ that leads to this result is the best estimate of $\hat{\sigma}_j$ for σ_j.

Partial Derivatives of Projection Equations

For equations (A5)

$$\bar{x}_i = F\left(\sigma_j\right) + e_i \qquad (j = 1, 2, 3)$$

$$\bar{y}_i = \overline{F}\left(\sigma_j\right) + e_i \qquad (i = 1, \ldots, n)$$

The partial derivatives of F and $\overline{F}$ with respect to σ_1, σ_2, and σ_3 are as follows. Let

$$p = \lambda_1 X + \mu_1 Y + \nu_1 Z$$

$$q = \lambda_2 X + \mu_2 Y + \nu_2 Z$$

$$r = \lambda_3 X + \mu_3 Y + \nu_3 Z$$

then

$$\frac{\partial F}{\partial \sigma_1} = \frac{c\left(\frac{\partial p}{\partial \sigma_1} r - \frac{\partial r}{\partial \sigma_1} p\right)}{r^2}$$

$$\frac{\partial F}{\partial \sigma_2} = \frac{c\left(\frac{\partial p}{\partial \sigma_2} r - \frac{\partial r}{\partial \sigma_2} p\right)}{r^2}$$

APPENDIX

$$\frac{\partial F}{\partial \sigma_3} = \frac{c\left(\frac{\partial p}{\partial \sigma_3} r - \frac{\partial r}{\partial \sigma_3} p\right)}{r^2}$$

$$\frac{\partial \overline{F}}{\partial \sigma_1} = \frac{c\left(\frac{\partial q}{\partial \sigma_1} r - \frac{\partial r}{\partial \sigma_1} q\right)}{r^2}$$

$$\frac{\partial \overline{F}}{\partial \sigma_2} = \frac{c\left(\frac{\partial q}{\partial \sigma_2} r - \frac{\partial r}{\partial \sigma_2} q\right)}{r^2}$$

$$\frac{\partial \overline{F}}{\partial \sigma_3} = \frac{c\left(\frac{\partial q}{\partial \sigma_3} r - \frac{\partial r}{\partial \sigma_2} q\right)}{r^2}$$

$$\frac{\partial p}{\partial \sigma_1} = \mu_1 X - \lambda_1 Y$$

$$\frac{\partial q}{\partial \sigma_1} = \mu_2 X - \lambda_2 Y$$

$$\frac{\partial r}{\partial \sigma_1} = \mu_3 X - \lambda_3 Y$$

$$\frac{\partial p}{\partial \sigma_2} = -\nu_1\left(X \sin \sigma_1 + Y \cos \sigma_1\right) - \left(\sin \sigma_2 \sin \sigma_3\right) Z$$

$$\frac{\partial q}{\partial \sigma_2} = -\nu_2\left(X \sin \sigma_1 + Y \cos \sigma_1\right) - \left(\sin \sigma_2 \cos \sigma_3\right) Z$$

$$\frac{\partial r}{\partial \sigma_2} = -\nu_3\left(X \sin \sigma_1 + Y \cos \sigma_1\right) + Z \cos \sigma_2$$

$$\frac{\partial p}{\partial \sigma_3} = \lambda_2 X + \mu_2 Y + \nu_2 Z = N$$

$$\frac{\partial q}{\partial \sigma_3} = -\left(\lambda_1 X + \mu_1 Y + \nu_1 Z\right) = -M$$

$$\frac{\partial r}{\partial \sigma_3} = 0$$

APPENDIX

Coordinate Transformation

Object space points and the position of the camera are initially identified in terms of geodetic latitude, longitude, and altitude above sea level. These data are obtained from maps of the photographed area and radar observations of the vehicle trajectory. In order to reference the data relative to the camera as described previously the earth centered geocentric coordinates of both the object space points and the vehicle position are computed by

$$\overline{X}_i = \left(R_i + h_i\right)\cos \Phi_i' \cos \Lambda_i$$

$$\overline{Y}_i = \left(R_i + h_i\right)\cos \Phi_i' \sin \Lambda_i$$

$$\overline{Z}_i = \left(R_i + h_i\right)\sin \Phi_i'$$

and

$$\Phi_i' = \Phi_i - 11'35.6635'' \sin 2\Phi_i + 1.1731'' \sin 4\Phi_i - 0.0025'' \sin 6\Phi_i$$

$$R_i = 6378.388(0.998320047 + 0.001683494 \cos 2\Phi_i - 0.000003549 \cos 4\Phi)$$

where

$i = 1$ for the vehicle position

$i = 2 \ . \ . \ . \ n+1$ for the object space points

In the preceding the $\overline{X}$ axis is in the equatorial plane pointing toward the Greenwich meridian, the $\overline{Y}$ axis 90^o east in the equatorial plane and the $\overline{Z}$ axis toward the north pole. A slight error is introduced by adding altitude to the earth's radius vector but this is negligible for the accuracy desired of this system.

The following transformation maps the geocentric coordinates into object space coordinates relative to the camera where the X axis points east, the Y axis north, and the Z axis toward the zenith.

$$\begin{bmatrix} X_{i+1} \\ Y_{i+1} \\ Z_{i+1} \end{bmatrix} = \begin{bmatrix} -\sin \Lambda_1 & \cos \Lambda_1 & 0 \\ -\cos \Lambda_1 \sin \Phi_1 & -\sin \Lambda_1 \sin \Phi_1 & \cos \Phi_1 \\ \cos \Lambda_1 \cos \Phi_1 & \sin \Lambda_1 \cos \Phi_1 & \sin \Phi_1 \end{bmatrix} \begin{bmatrix} \overline{X}_{i+1} - \overline{X}_1 \\ \overline{Y}_{i+1} - \overline{Y}_1 \\ \overline{Z}_{i+1} - \overline{Z}_1 \end{bmatrix}$$

This transformation is obtained by a positive rotation about the $\overline{Z}$ axis through an angle of $90^o + \Lambda_1$ followed by a positive rotation about the new X axis through an angle of $90^o - \Phi_1$.

REFERENCES

1. Fraser, L. W.; and Ostrander, R. S.: Photographic Determination of the Orientation of a Rocket. Phot. Eng., vol. 1, Oct. 1950, pp. 105-118.

2. Kinder, Floyd A.: Evaluation of a Single-Camera Method for Determining Aircraft Position and Attitude. NAVORD Rept. 5603, U.S. Naval Ord. Test Station, Sept. 1, 1957.

3. Strand, Otto Neall: Mathematical Methods Used To Determine the Position and Attitude of an Aerial Camera. NAVORD Rept. 5333, U.S. Naval Test Station, Mar. 1956.

4. Darnell, Wayne L.; Henning, Allen B.; and Lundstrom, Reginald R.: Flight Test of a 15-Foot-Diameter (4.6-Meter) 120^{o} Conical Spacecraft Simulating Parachute Deployment in a Mars Atmosphere. NASA TN D-4266, 1967.

5. Whitlock, Charles H.; Bendura, Richard J.; and Coltrane, Lucille C.: Performance of a 26-Meter-Diameter Ringsail Parachute in a Simulated Martian Environment. NASA TM X-1356, 1967.

6. Hogge, John E.: Three Ballistic Camera Data Reduction Methods Applicable to Reentry Experiments. NASA TN D-4260, 1967.

TABLE I.- GEODETIC COORDINATES AND ALTITUDE OF IDENTIFICATION POINTS

[See fig. 2]

Point	Latitude	Longitude	Altitude	
			ft	m
2	33°13.8'	106°26.5'	4050	1234
4	33°17.9'	106°31.9'	8358	2548
5	33°16.8'	106°23.6'	4075	1242
6	33°40.3'	106°58.7'	4912	1497
7	33°29.0'	107° 7.8'	4500	1372
8	33° 9.0'	107°11.0'	4500	1372
9	33°13.8'	106°38.4'	7600	2316
10	33°20.0'	106°30.5'	7900	2408
11	33°36.6'	106°21.3'	8114	2473
12	34°15.3'	106°53.9'	4750	1448

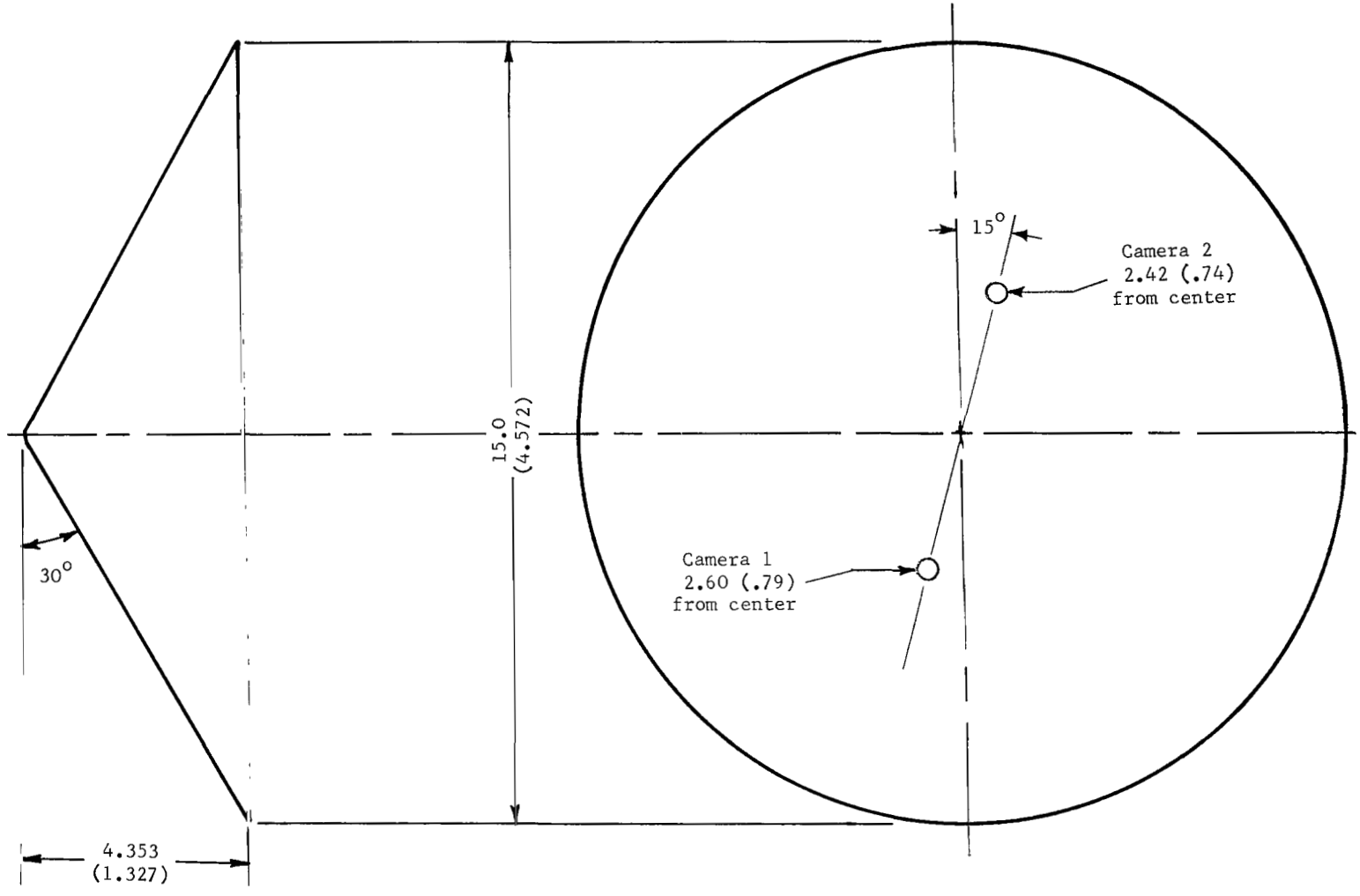

Figure 1.- Sketch of aeroshell, side and rear view. All dimensions are in feet (meters).

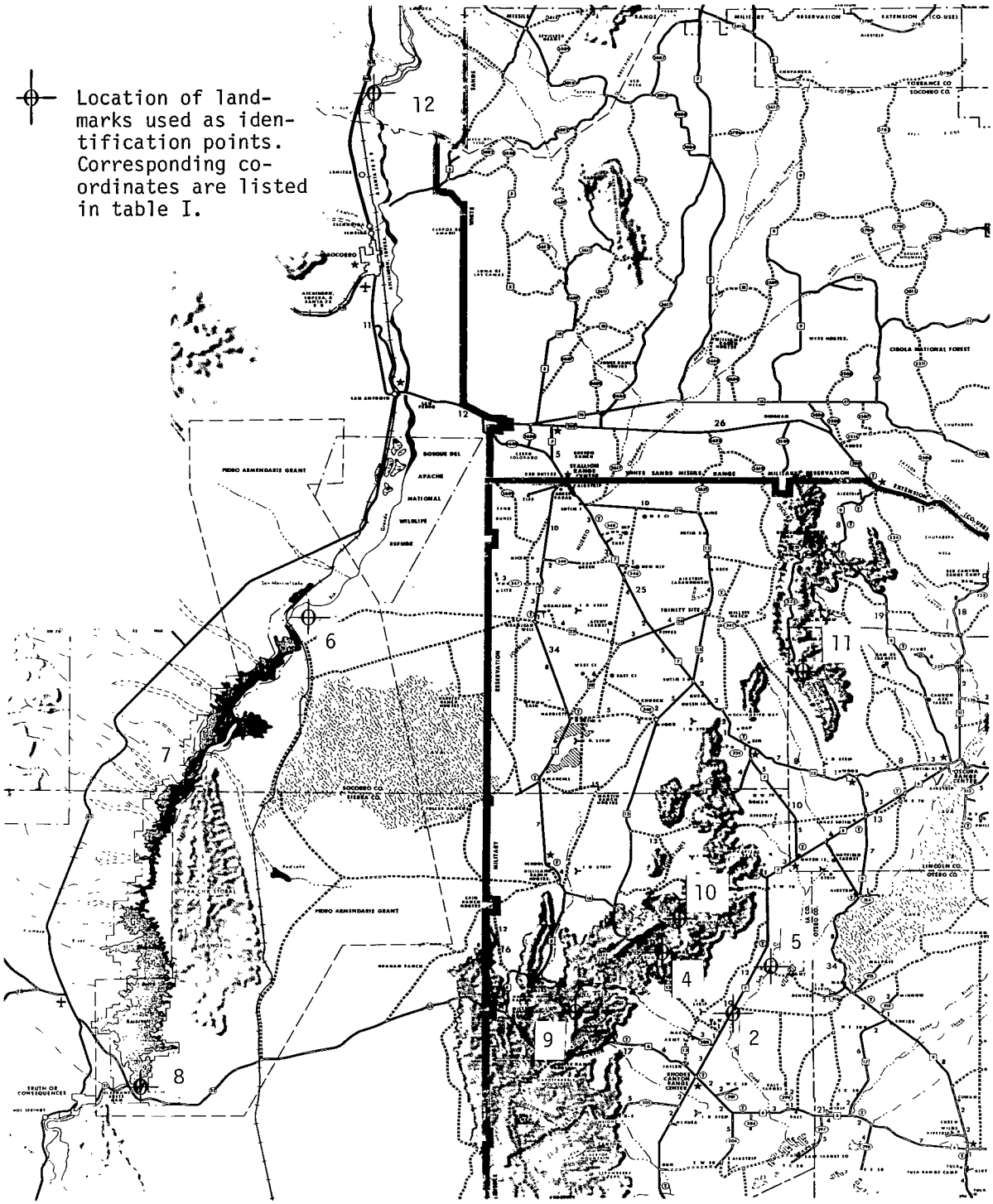

Figure 2.- Topographical map showing location of identification points. L-67-8703

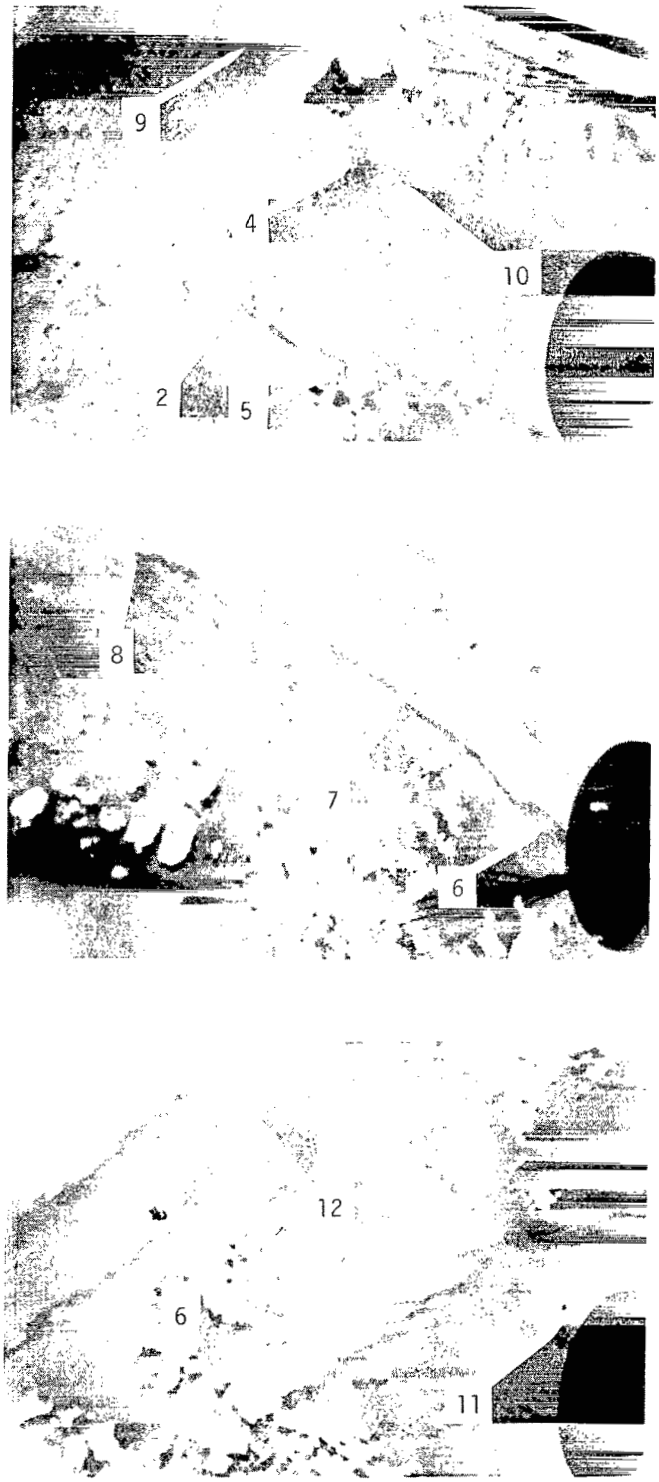

Figure 3.- Typical photographs with landmark identification points indicated. (See table I.) L-67-8704

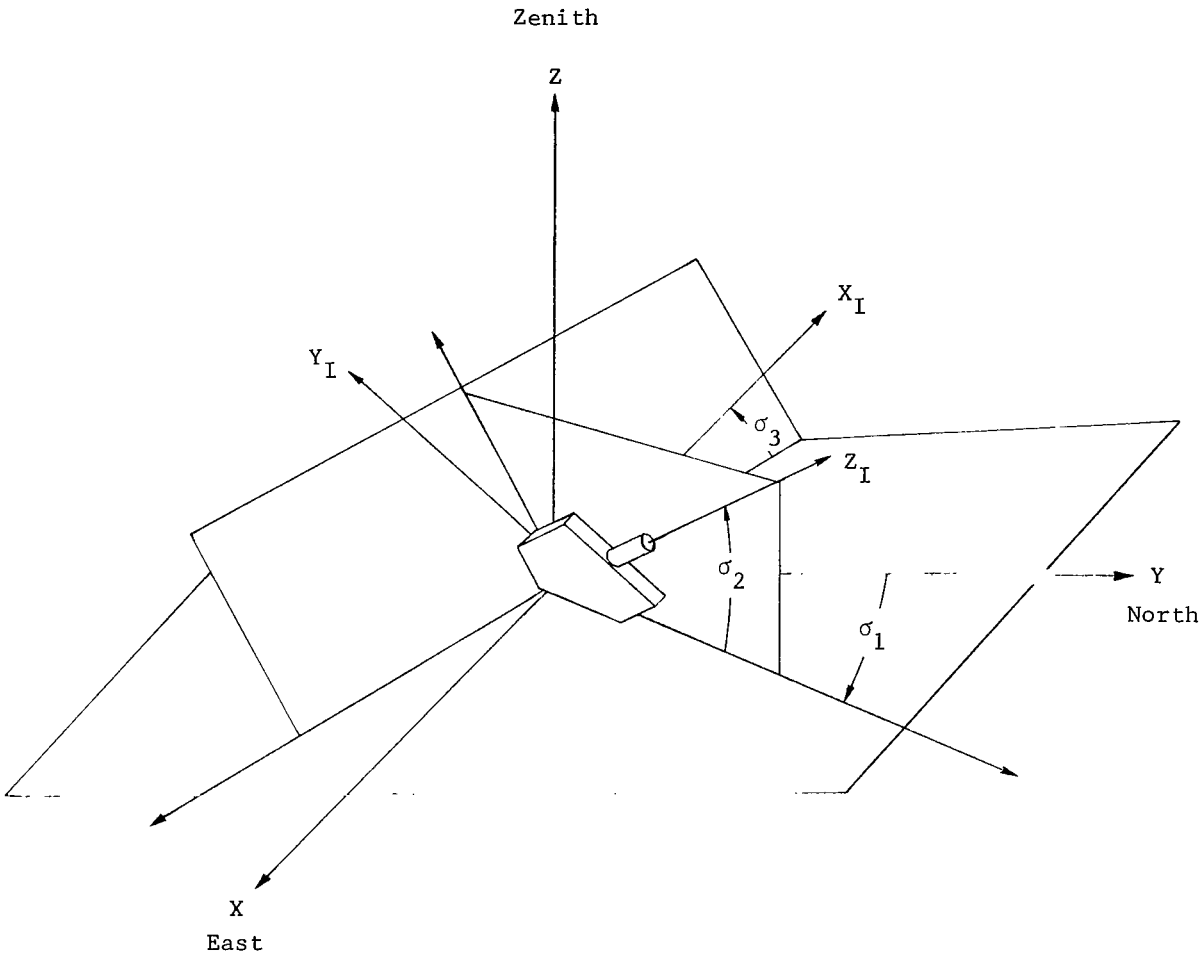

Figure 4.- Camera rotations.

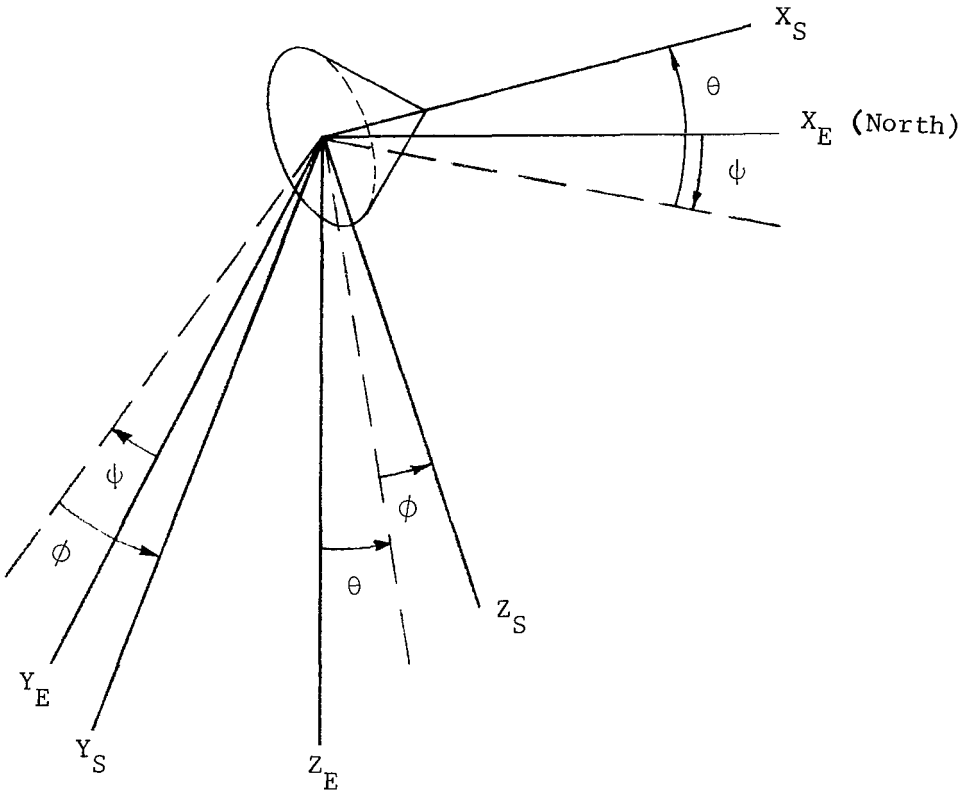

Figure 5.- Spacecraft axes system.

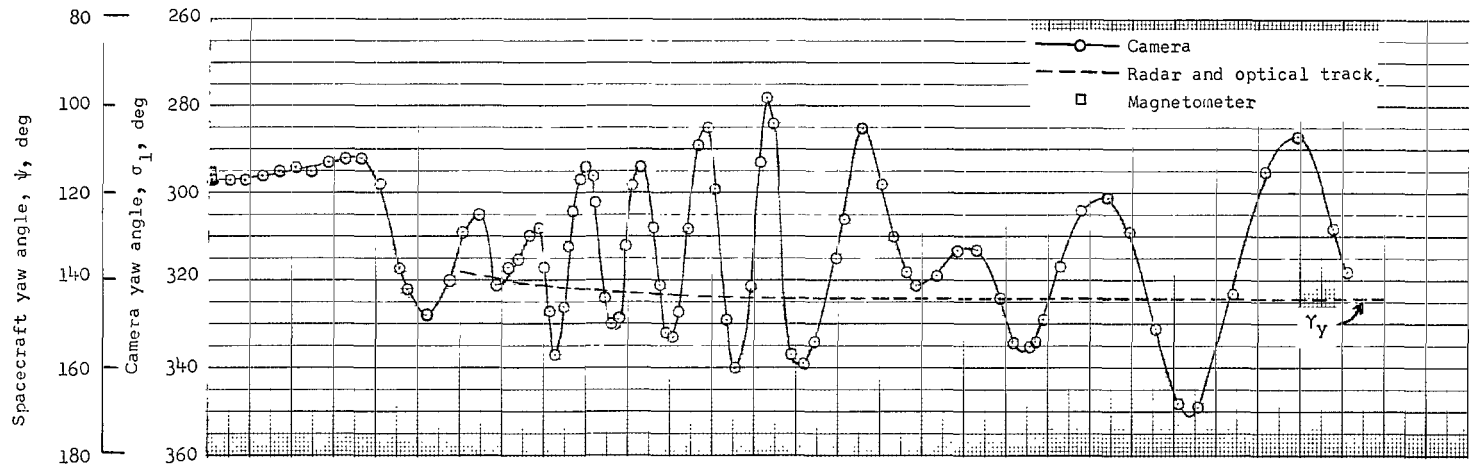

(a) Camera 1.

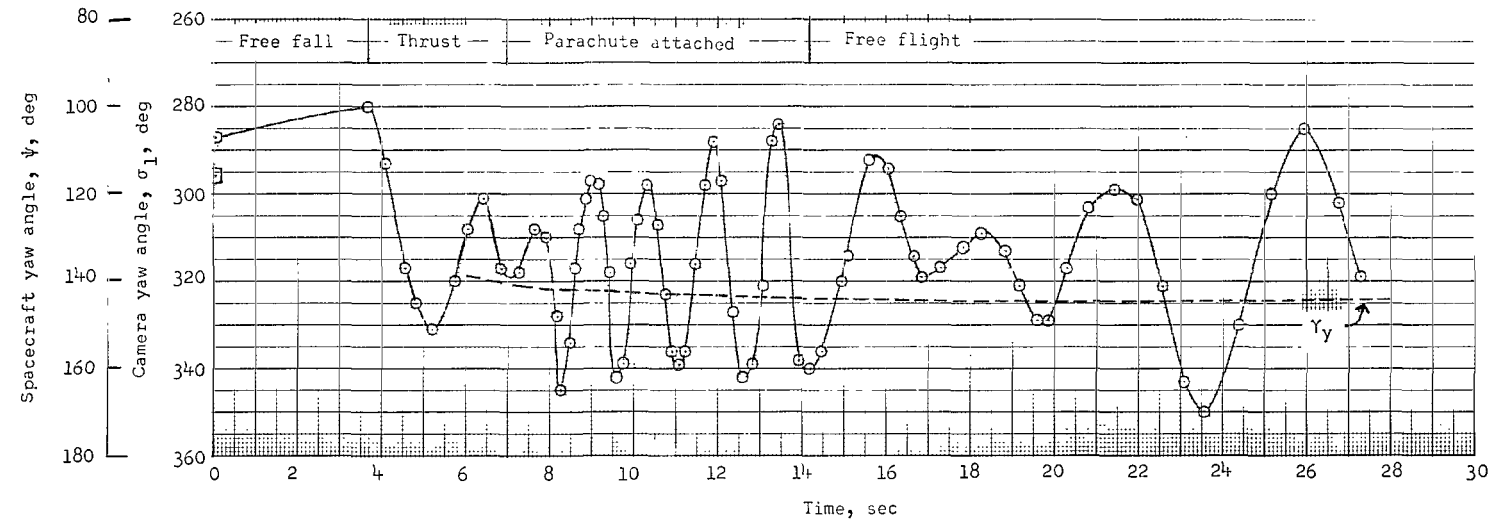

(b) Camera 2.

Figure 6.- Yaw-angle variation with time compared with ground track data γ_y.

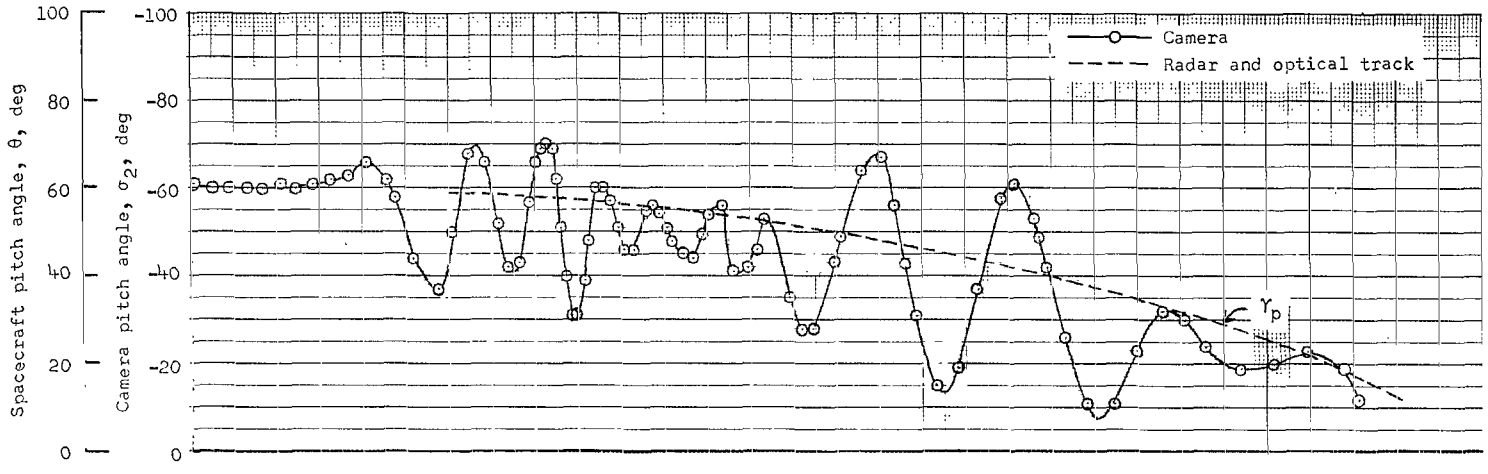

(a) Camera 1.

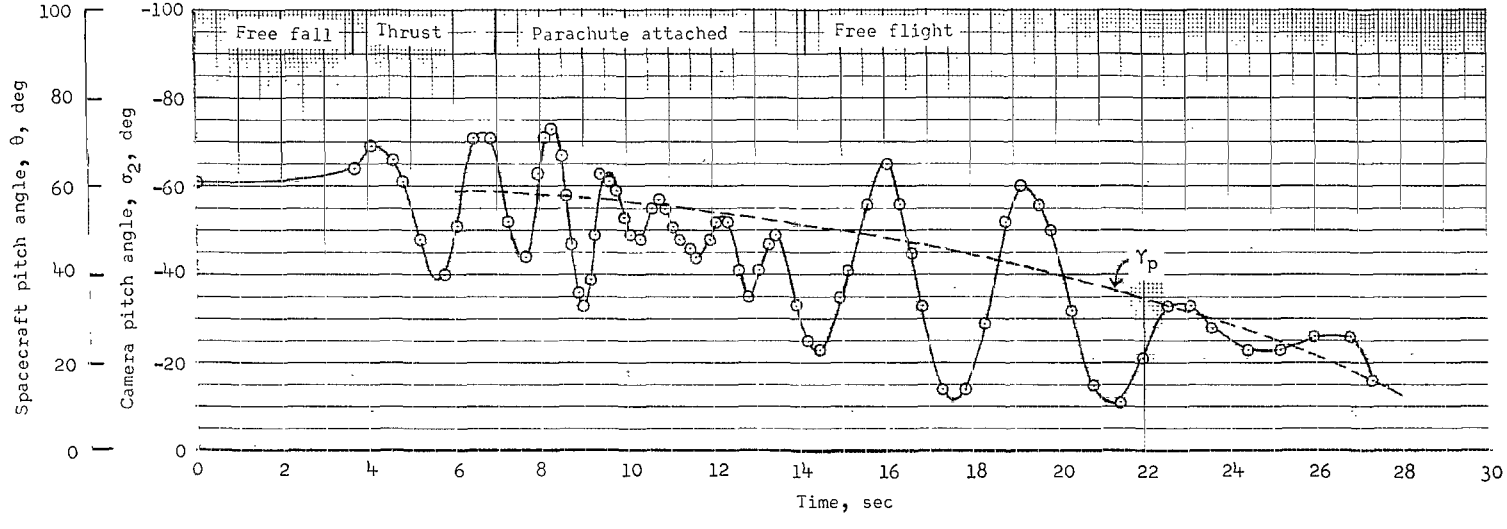

(b) Camera 2.

Figure 7.- Pitch-angle variation with time compared with ground track data γ_p.

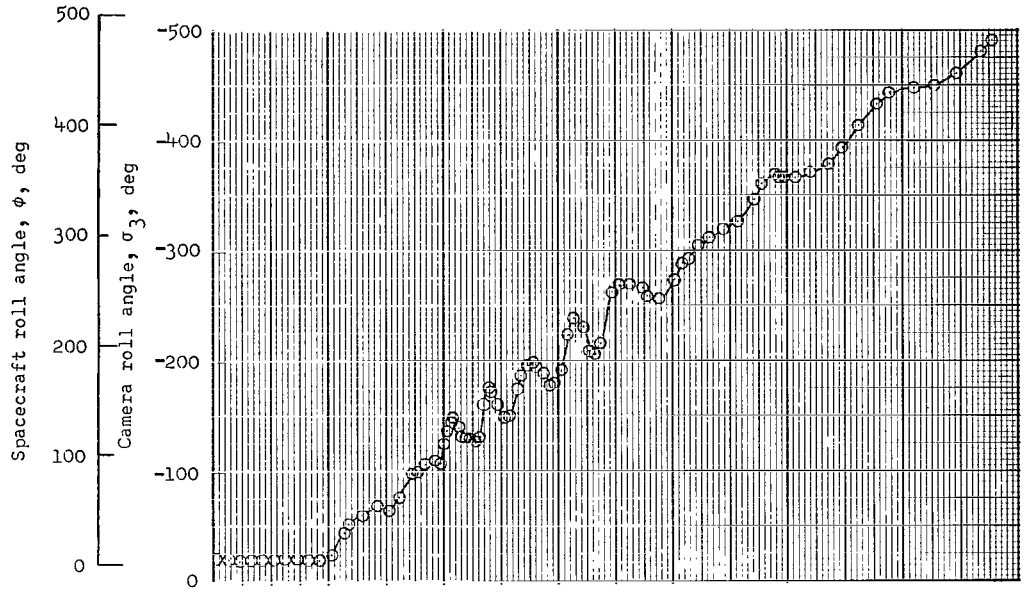

(a) Camera 1.

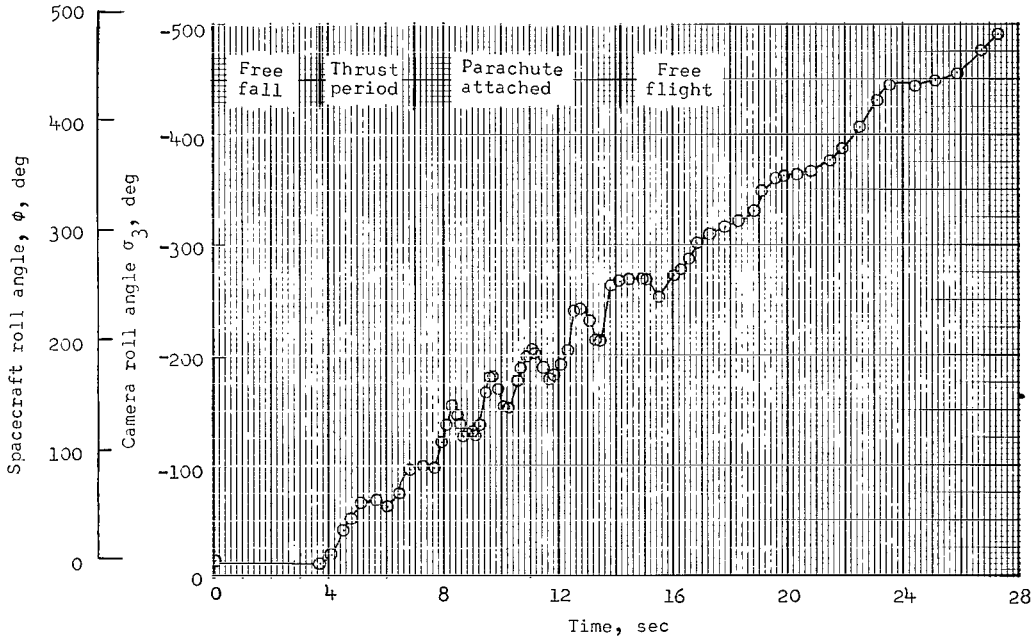

(b) Camera 2.

Figure 8.- Roll-angle variation with time.

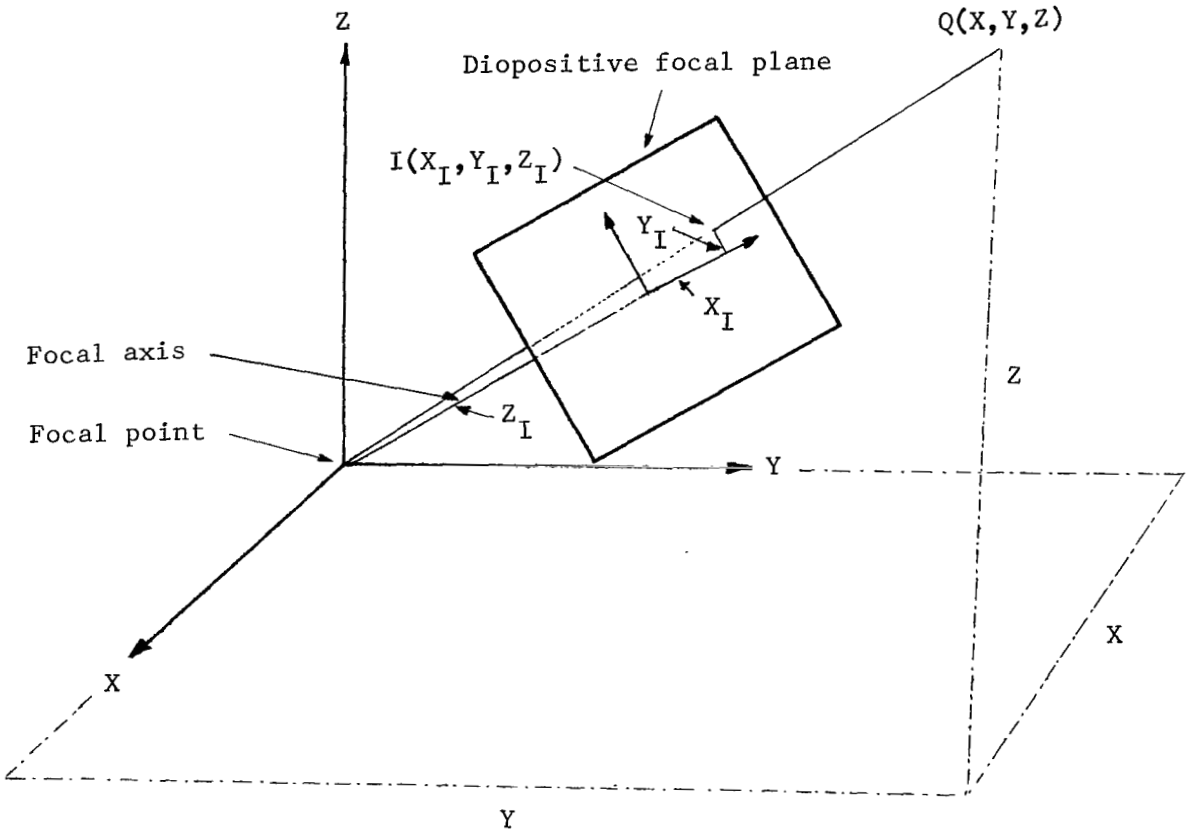

Figure 9.- Axis systems relating image space and object space.

"The aeronautical and space activities of the United States shall be conducted so as to contribute . . . to the expansion of human knowledge of phenomena in the atmosphere and space. The Administration shall provide for the widest practicable and appropriate dissemination of information concerning its activities and the results thereof."

—NATIONAL AERONAUTICS AND SPACE ACT OF 1958

NASA SCIENTIFIC AND TECHNICAL PUBLICATIONS

TECHNICAL REPORTS: Scientific and technical information considered important, complete, and a lasting contribution to existing knowledge.

TECHNICAL NOTES: Information less broad in scope but nevertheless of importance as a contribution to existing knowledge.

TECHNICAL MEMORANDUMS: Information receiving limited distribution because of preliminary data, security classification, or other reasons.

CONTRACTOR REPORTS: Scientific and technical information generated under a NASA contract or grant and considered an important contribution to existing knowledge.

TECHNICAL TRANSLATIONS: Information published in a foreign language considered to merit NASA distribution in English.

SPECIAL PUBLICATIONS: Information derived from or of value to NASA activities. Publications include conference proceedings, monographs, data compilations, handbooks, sourcebooks, and special bibliographies.

TECHNOLOGY UTILIZATION PUBLICATIONS: Information on technology used by NASA that may be of particular interest in commercial and other non-aerospace applications. Publications include Tech Briefs, Technology Utilization Reports and Notes, and Technology Surveys.

Details on the availability of these publications may be obtained from:

SCIENTIFIC AND TECHNICAL INFORMATION DIVISION

NATIONAL AERONAUTICS AND SPACE ADMINISTRATION

Washington, D.C. 20546